THE ASTROPHYSICAL JOURNAL, 325:207–217, 1988 February 1

GRAVITATIONAL LIGHT BENDING NEAR NEUTRON STARS. I. EMISSION FROM COLUMNS AND HOT SPOTS

H. RIFFERT[1] AND P. MÉSZÁROS
Astronomy Department, Pennsylvania State University
Received 1986 November 24; accepted 1987 July 22

ABSTRACT

We calculate the beam shapes, pulse profiles, and spectral transmission function at infinity for the radiation originating in columns or hot spots on slowly rotating neutron stars, represented by the Schwarzschild metric. These are used for models for binary accreting pulsars and may apply to isolated neutron stars as well. We discuss the shadowing effects and their interplay with the frequency changes as a function of the observer angle. We give the observed bolometric beam shapes and pulse profiles as a function of radius, as well as observed pulse-phase spectra and frequency-dependent pulse profiles, for various types of source functions at the surface. The more realistic accretion (or emission) column geometry used indicates that these may show a larger degree of modulation than was previously thought, as compared to hot spots. The observational implications for X-ray–emitting pulsars are discussed.

Subject headings: gravitation — pulsars — relativity — stars: neutron — X-rays: binaries

I. INTRODUCTION

Gravitational light bending is expected to occur near neutron stars whose radii are not much greater than the Schwarzschild radius. For most current models of the equation of state (see Shapiro and Teukolsky 1983) the ratio of the stellar radius R to the Schwarzschild radius $R_S = 2GM/c^2$ is approximately in the range $2 \leq R/R_S \leq 4$, in which case the photon orbits will significantly deviate from the flat-space case (see Misner, Thorne, and Wheeler 1973). This is of great observational importance in the interpretation of both rotation-powered and accretion-powered pulsars since a very large body of the data consists of pulse profiles and timing information, and much, if not most, of this radiation is expected to arise from the stellar surface or very close to it. Recently, Pechenick, Ftaclas, and Cohen (1983) and Ftaclas, Kearney, and Pechenick (1986) have investigated the influence of these effects on the beaming of the bolometric (frequency-integrated) radiation from a hot spot on the surface of a slowly rotating neutron star in the limit where the Schwarzschild metric is applicable. A general flattening of the light curves was found, and, for extremely relativistic stars, a certain fraction of the radiation observed at infinity is beamed, even for an assumed isotropic input at the surface. These results may apply to some polar-cap models of rotation-powered pulsars (e.g., Cheng and Ruderman 1980; Helfand, Chanan, and Novick 1980; Arons 1981) and to polar-cap (or slab) models of accretion-powered X-ray pulsars, e.g., such as one would obtain if the deceleration of the infalling matter occurs through binary particles encounters in the denser parts of the atmosphere (Zel'dovich and Shakura 1969; Alme and Wilson 1973; Mészáros *et al.* 1983; Harding *et al.* 1984). The emission surface in these models coincides essentially with the stellar surface.

In this paper, we investigate a different set of problems associated with the fact that a significant fraction, or perhaps most of the radiation, may in some cases originate from regions which are not part of the stellar surface. For accreting pulsars, it would be relevant for the case when the infalling matter decelerates at some distance above the surface due to shocks or radiation pressure (which may be more prevalent at higher luminosities). In this case, one has an accretion "column" rather than a polar cap or hot spot, and, as a reasonable approach to this type of emission region, we consider a radiating cone which emits only from its sides, but not from the top (Davidson 1973; Basko and Sunyaev 1976; Wang and Frank 1981; Kirk 1985). A review of the various arguments for hot spots or columns in accreting pulsars is given by Mészáros (1984). In the general relativistic treatment of the emission from a column, there appear two new, qualitatively different effects, which are not present in polar-cap or hot-spot models. First, the frequency redshift is different for radiation arising from different heights, and a treatment of the frequency-integrated (bolometric) luminosity does not reveal the full complexity of the situation. Second, the star and the elevated emission region (or accretion column) will both produce some shadowing of the light rays, as they proceed on their curved paths, and this effect depends on the emission height (or frequency) and on the direction of observation.

In § II, we present the formalism of frequency-dependent transfer in a Schwarzschild metric. This is specialized in Appendix A to the situation where one is considering an accretion column or a raised emission region. For completeness, we discuss also the case of a surface hot spot in Appendix B. We concentrate in particular on the observational quantities that are most often measured, e.g., the spectral photon flux and the total apparent flux at infinity. In § III, results are presented for the frequency-integrated beam shapes and expected pulse profiles in the case of emission columns for various stellar radii and for various different orientations of the rotation and column axes with respect to the observational line of sight. We present calculations using an isotropic input angular distribution at the source and discuss the changes introduced by more beamed input distributions such as are expected from scattering atmospheres. The results for the columns are then compared with the hot-spot beam shapes and pulse profiles. Some of the shadowing effects due to the more complex column geometry are already quite apparent for the bolometric flux. In § IV, we discuss the frequency dependence of the observed flux,

[1] On leave from Max-Planck-Institut für Astrophysik, Garching, FRG.

assuming that the input spectrum is a delta function in frequency. We discuss the observed spectral flux, and the observed pulse shapes from accretion columns as a function of frequency, for varying stellar radii and column dimensions. The observational implications of our results, as well as a discussion of their physical significance, are given in § V.

II. FORMALISM

We assume that the central object is slowly rotating ($\Omega R_S \ll c$) and that the gravitational effects of the external flow are negligible compared to those of the central object whose radius is R. The Schwarzschild metric (with coordinates t, r, Θ, Φ) is then appropriate, with Schwarzschild radius $R_S = 2GM/c^2$, where M is the stellar mass. The propagation of the radiation near the star can be described by a relativisitc transport equation for an invariant photon distribution function f, which was derived by Lindquist (1966) in its general form. For the stationary ($\partial/\partial t = 0$), rotationally symmetrical case ($\partial/\partial\Phi = 0$), the transport equation with respect to an orthonormal basis can be derived by the method of Rifferent (1986),

$$A\mu \frac{\partial f}{\partial r} + \frac{(1-\mu^2)^{1/2}}{r} \cos\phi \frac{\partial f}{\partial \Theta} + \left(A - r\frac{dA}{dr}\right)\frac{1-\mu^2}{r}\frac{\partial f}{\partial \mu} - \frac{(1-\mu^2)^{1/2}}{r}\sin\phi \operatorname{ctg}\Theta \frac{\partial f}{\partial \phi} - \frac{dA}{dr}\mu\nu\frac{\partial f}{\partial \nu} = 0 . \quad (1)$$

Measuring the radial coordinate in units of R_S, one has $A = (1 - 1/r)^{1/2}$. The propagation direction of a photon is characterized by the unit vector

$$\boldsymbol{n} = [\mu, (1-\mu^2)^{1/2}\cos\phi, (1-\mu^2)^{1/2}\sin\phi] ,$$

which defines the angles μ and ϕ (actually μ is the cosine of the angle between $\boldsymbol{n}$ and the radial direction). Together with ν, the photon frequency, these three parameters characterize the photon four-momentum.

We assume that the photon is emitted at a point $Q = (r_0, \Theta_0, \Phi_0)$ with frequency ν_0, in the direction (μ_0, ϕ_0). It is observed at the point $P = (r, \Theta, \Phi)$ with the corresponding four-momentum quantities (ν, μ, ϕ) (see Fig. 1). In the limit $r \to \infty$, the spectral flux observed is given by (we use $h = c = 1$ throughout)

$$F_\nu = \iint_{4\pi} I_\nu \mu\, d\mu\, d\phi = \nu^3 \iint_{4\pi} f \mu\, d\mu\, d\phi , \quad (2)$$

where I_ν stands for the specific intensity, and all quantities in equation (2), including the solid angle of integration, are measured at the observer. The function f is constant along the characteristics of the transport equation (1). The equations for the characteristics may be used, therefore, to express the integral (2) in terms of the emission quantities μ_0, ϕ_0, etc.:

$$F_\nu = \nu^3 \iint_{4\pi} f_0 D(\mu, \phi; \mu_0, \phi_0)\mu\, d\mu_0\, d\phi_0 , \quad (3)$$

where D is the Jacobian of this transformation, f_0 stands for the distribution function as a function of the variables r_0, Θ_0, μ_0, ϕ_0, ν_0, and the integral over 4π is now carried out over the transformed domain in the emission region itself.

The characteristics of equation (1), the first three of which are immediately integrable, are

$$\frac{r}{A}(1-\mu^2)^{1/2} = b = \frac{r_0}{A_0}(1-\mu_0^2)^{1/2} , \quad (4a)$$

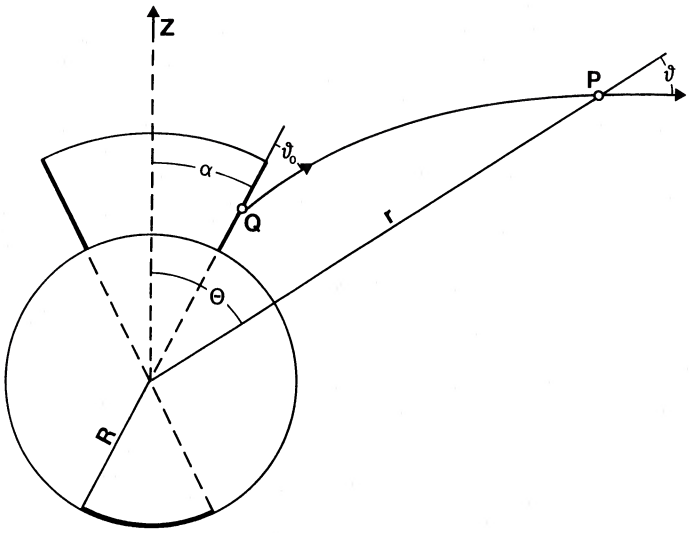

FIG. 1.—Geometry of the situation, showing coordinates of the emission point $Q(r_0, \Theta_0, \Phi_0)$, of the observation point $P(r, \Theta, \Phi)$, and photon four-momentum quantities μ_0, ϕ_0, ν_0 and μ, ϕ, ν, respectively, where $\mu = \cos(\theta)$ (note that the azimuthal angles Φ, ϕ, Φ_0, and ϕ_0 are not explicitly indicated). Also shown are the column (*top*) or cap (*bottom*) configurations, of half-opening angle α.

$$\sin\Theta \sin\phi = \sin\Theta_0 \sin\phi_0 , \quad (4b)$$

$$\nu A = \nu_0 A_0 , \quad (4c)$$

$$\frac{d\Theta}{dr} = b\frac{\cos\phi}{\mu r^2} . \quad (4d)$$

Here, $A_0 = (1 - 1/r_0)^{1/2}$, equation (4a) defines the relativistic impact parameter b (see Misner, Thorne, and Wheeler 1973), and equation (4c) gives the usual redshift relation. Integrating equation (4d) with the help of equations (4a) and (4b) yields the result

$$\cos\Theta = \cos\Theta_0 \cos K - \cos\phi_0 \sin\Theta_0 \sin K , \quad (4e)$$

where the quantity $K(r, r_0, \mu_0)$ is the angle between the radius vector pointing toward the emission point $Q(r_0)$ and the radius vector point to the observation point $P(r)$ for a photon emitted with μ_0. In the following, we consider $r_0 > 1.5$, in which case any outwardly directed photon ($\mu_0 > 0$) is able to escape to infinity. Here $K(r, r_0, \mu_0)$ is given by

$$K(r, r_0, \mu_0) = b\int_{r_0}^{r}\left[x^2 - b^2\left(1 - \frac{1}{x}\right)\right]^{-1/2}\frac{dx}{x} + Q(r_0, \mu_0) , \quad (5a)$$

where

$$Q(r_0, \mu_0) = \begin{cases} 0 , & \mu_0 \geq 0 , \\ 2b\displaystyle\int_{r_m}^{r_0}\left[x^2 - b^2\left(1 - \frac{1}{x}\right)\right]^{-1/2}\frac{dx}{x} , & \mu_0 < 0 , \end{cases} \quad (5b)$$

and r_m is a solution of the cubic equation

$$r_m^3 - b^2(r_m - 1) = 0 . \quad (6)$$

Here, r_m is the distance of minimum approach of the photon to the star, meaningful in the case where the photon has been emitted somewhere above the star and in a downward direc-

tion. A solution for positive r_m exists only if

$$b^2 > \frac{27}{4} \quad \text{or} \quad \mu_0 > -\left[1 - \frac{27}{4r_0^2}\left(1 - \frac{1}{r_0}\right)\right]^{1/2}. \qquad (7)$$

This is a necessary condition for the validity of equation (5b), otherwise the photon falls back onto the star. From the relations (4) and (5), the Jacobian D in the flux integral (3) can be calculated for any shape of the emitting surface.

III. RESULTS: BOLOMETRIC ANGULAR DEPENDENCE

a) Column: Frequency-Integrated Emission

The frequency-integrated emission from the sides of an accretion column is calculated in detail in Appendix A. Shadowing effects are taken care of by the appropriate choice of the integration region S_0 and of the initial photon distribution at the emission surface, I_0 (see eqs. [A12]–[A14]). We further assume that the top of the column does not radiate. This is considered reasonable for accretion columns in high-luminosity pulsars, where, due to the dynamical structure of the emission region, most of the radiation is expected to be radiated sideward (in the upward direction the opacity is larger and photons have to diffuse upstream). In all cases presented here, we have taken I_0 to be independent of the radius r_0 and of the emission angles ϕ_0 and μ_0, i.e., I_0 is assumed to show an isotropic emission pattern.

In order to get an idea of the general emission properties of a radiating column we first consider the propagation of a single light ray emitted at $r = r_0$ with $\phi_0 = 0$ from the side of a column with an opening half-angle α centered on $\Theta = 0$. For a fixed stellar radius R there is then an emission radius $r_0 = R_\pi$ such that a light ray emitted from that height is tangential to the stellar surface at some point and escapes to infinity into the direction $\Theta = \pi$. This is a preferred direction because, for a column emitting from its whole surface, a large fraction of the area contributes to the observed flux: for symmetry reasons the visible parts of the column are complete ring areas whereas for other observation angles only some spotlike parts of the surface might be visible. The above radius R_π is a function of R and α, and this function is shown in Figure 2 (note that for $\alpha = 0$, R_π is identical with the focal length defined in the paper of Ftaclas, Kearney, and Pechenick 1986). Light rays emitted at lower radii ($r_0 < R_\pi$) are not visible at $\Theta = \pi$ (the reason for that is that rays emitted at $\mu_0 < \mu_R$ with μ_R defined in equation [A2] are absorbed by the star; μ_R is monotonically decreasing with r_0 and the deflection angle K [see eq. (5)] decreases monotonically with μ_0). The angular dependence of the observed flux from a radiating column will thus depend on whether its upper radius R_c lies within the distance R_π or not. Figure 3 shows an example of a single column with $\alpha = 5°$ on a star with $R = 3R_S$ for various column upper radii R_c; the corresponding value of R_π is $R_\pi = 3.94R_S$. For $R_c < R_\pi$, the emission from the column will be obscured completely by the star for large observation angles Θ. If $R_c > R_\pi$, parts of the column are still visible at $\Theta = \pi$, and, due to the large visible area, the flux is strongly increased.

In the following example (Figs. 4 and 5) we have considered emitting columns with various combinations of lower and upper radii R and R_c, respectively. We have performed calculations for stellar radii $R/R_S = (1.7, 2.0, 2.5, 3.0, 3.5, 4.0, 5.0, 10.0, 100.0)$, and have chosen in each case R_c such that the total emitted luminosity (see eq. [A16]) remained the same. The normalization was chosen such that, for $R = 2$, $R_c = 2.2$. For larger radii, $\Delta R/R$ is less than 10%, and, for smaller radii, it is more, the values being $R_c = (1.95, 2.20, 2.65, 3.12, 3.60, 4.09, 5.07, 10.03, 100.003)$. The constant luminosity constraint has been chosen arbitrarily. One can argue that the luminosity (or flux) is a given observable, whereas what we do not know is the stellar radius and column radii. Since the luminosity depends on the emitting area, for the various R we choose the R_c that would give the same emitted luminosity. That is, however, by no means a necessary choice.

The results shown in Figure 4 represent the beam function for the emission from one pole only, including shadowing effects by the star. For some particular observers who sample

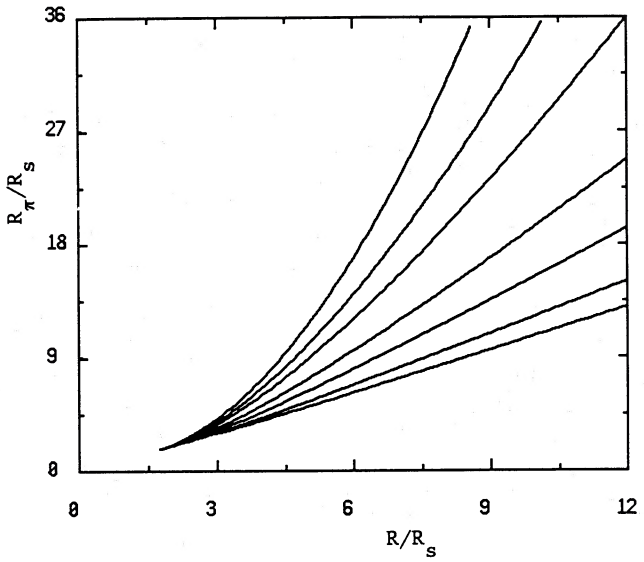

FIG. 2.—Generalized focal radius R_π as a function of stellar radius and column opening half-angle α. Values of α are (from top to bottom) 0°, 5°, 10°, 20°, 30°, 45°, 60°.

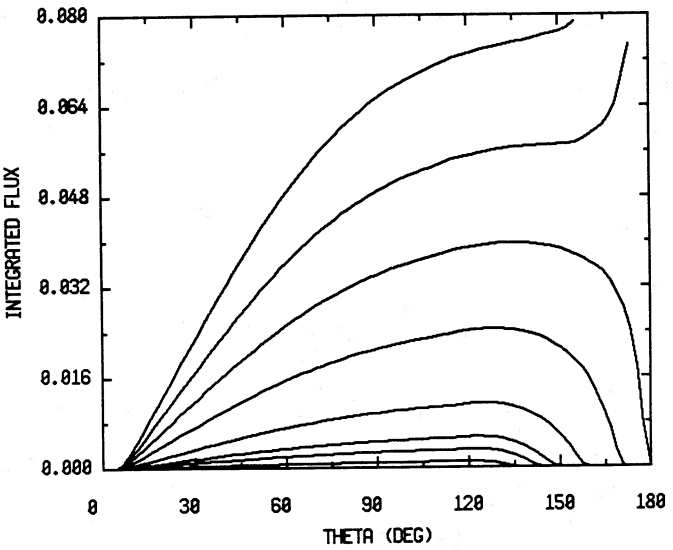

FIG. 3.—Column bolometric beam shape for an isotropic input intensity from a single column on top of a star with a radius $R = 3$, for various upper radii R_c. Ordinate shows normalized flux for an observer at infinity and the abscissa gives the observation angle Θ in degrees. The values of R_c are R_c = 3.03, 3.09, 3.15, 3.30, 3.60, 3.90, 4.20, 4.50. The column half-angle α is 5°, and $R_\pi = 3.94$. Radii are in Schwarzschild units.

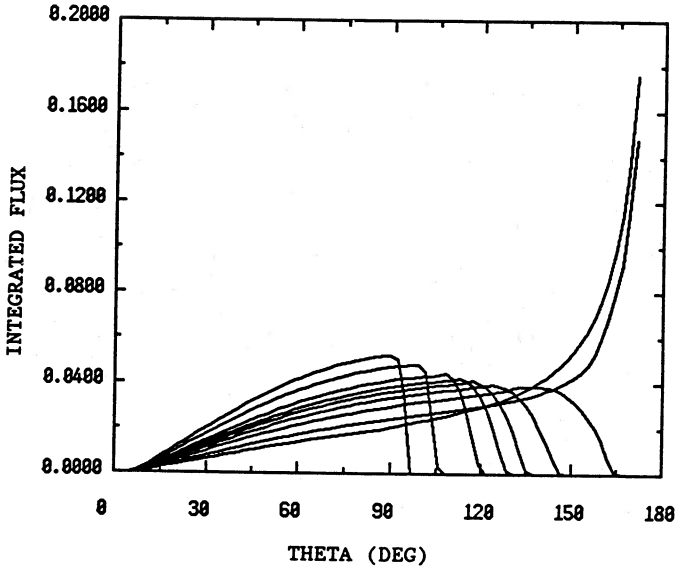

FIG. 4.—Column bolometric beam shape for an isotropic input intensity from surface of sides of column, extending between stellar radius R and an upper radius R_c. Values shown are (*see text*) R = 1.7, 2., 2.5, 3., 3.5, 4., 5., 10., 100.. Beaming pattern shown is for one pole with $\alpha = 5°$. Corresponding values of R_c and R_π are R_c = 1.95, 2.20, 2.65, 3.12, 3.60, 4.09, 5.07, 10.03, 100.003; R_π = <1.7, 2.04, 2.87, 3.94, 5.21, 6.66, 10.05, 34.72, 943.72.

$\Theta = 0$, this is also a light curve. For two poles, the beaming function is obtained from the one-pole beaming function by reflecting about 90° and taking into account any possible shadowing due to the second pole. The half-opening angle α of the column was again taken to be 5°. In Figure 5, we show the more general pulse profiles arising from such a two-pole configuration due to spinning of the neutron star, as a function of the spin phase $2\pi\Phi_*$, for various values of the observer aspect angles i_1, i_2 indicated along the top of the graph. Here, i_1 is the angle between the line of sight and the rotation axis and i_2 is the angle between the rotation axis and the magnetic or column axis. These angles are related to the observation angle Θ by

$$\cos(\Theta) = \cos(i_1)\cos(i_2) + \sin(i_1)\sin(i_2)\cos(2\pi\Phi_*) . \quad (8)$$

As seen from Figure 4 the emission is beamed strongly backward ($\Theta \approx \pi$) for $R < 2R_S$ (the lowest two curves), because in those cases the column extends above the radius R_π. For the remaining curves, we always have $R_c < R_\pi$, and therefore the columns are invisible at large observation angles. The actual cutoff angle where the flux goes to zero decreases with increasing stellar radius and approaches the limiting values $\alpha + \pi/2$ for less relativisitic configurations ($R > 10R_S$). Note that there is no emission for $\Theta < \alpha$ since the top of the column does not radiate, only the sides. In the interval $\alpha \leq \Theta < \pi/2$ the fluxes increase in a way similar to the "classical" (i.e., nonrelativistic) limb-darkening law $F \propto \sin\Theta$. The pulse shapes of Figure 5 show for the nonrelativistic limit (large radii) a smooth, low-modulation pulse, with "peaks" present at those phases where, for a particular set of viewing angles, one can see both columns simultaneously. For $i_1 = i_2 = 45°$ this occurs in the nonrelativistic limit near $\Theta = \pi/2$, where the flux jumps to twice the value, since one sees fully both columns. As the configurations become more relativistic, the width of these flat-topped peaks increases, due to increased bending of the light rays. For $R < 2R_S$, corresponding to a column model with $R_c > R_\pi$, the beaming has become essentially backward, and the peaks appear at phase zero, rather than near phase 0.5 as in the nonrelativistic case. The effect of varying a different parameter, such as the column height while leaving the radius constant is shown in Figure 6, where the pulse shapes corresponding to the beam shapes of Figure 3 are shown.

b) Caps: Frequency-Integrated Emission

We consider now the case of an emitting polar cap. That is, the situation where the emission arises from a portion of the

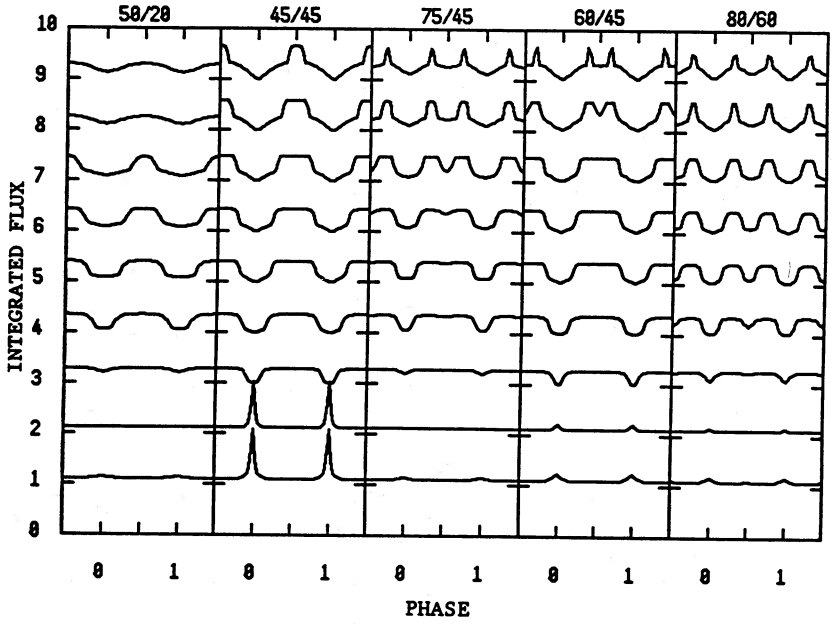

FIG. 5.—Column bolometric pulse shapes for two poles, for an isotropic emission function and a beam shape as given in Fig. 4. Ordinate gives normalized flux seen by an observer at infinity, for nine radii given in Fig. 4 in ascending order, bottom to top. Numbers along the top give the viewing angles i_1/i_2. Abscissa is pulse phase $2\pi\Phi_*$.

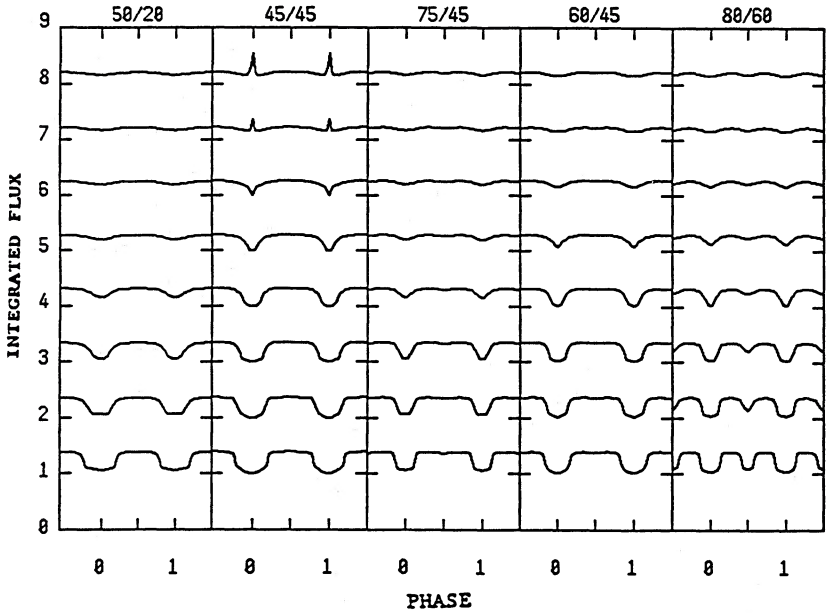

FIG. 6.—Column bolometric pulse shapes for two poles, isotropic injection function, $R = 3R_S$ and variable column height R_c as in Fig. 3

surface of the star around the magnetic poles, from a constant radius $r_0 = R$ rather than from a range of radii, as in the case of the accretion columns of § III*a*. In this case, the calculations are somewhat simpler (see Pechenick, Ftaclas, and Cohen 1983 and Appendix B). There is no shadowing by the star (for $r_0 = R > 1.5$), nor by the other pole. We have again used an opening half-angle α of 5° and an intrinsic beam function which is isotropic. The corresponding beam functions for a set of stellar radii have been discussed in detail by Pechenick, Ftaclas, and Cohen (1983). A flattening of the beam shape is obtained if R is reduced from large values to $R \approx 1.8R_S$ (for $\alpha < 10°$), and for smaller configurations a certain fraction of the flux is beamed into the backward direction ($\Theta \approx \pi$). However, the degree of backward beaming is less than in the column case, due to the fact that in the caps the flux is mainly emitted upward, rather than sideways as in the columns. The cap pulse shapes are presented in Figure 7 for the same set of radii as in the column case (Figs. 4 and 5). They show a smooth variation which is more modulated than the smooth component of the columns (as already found in the flat-space limit; see Nagel 1981 and Mészáros and Nagel 1985). However, the cap pulses do not show the extra flat-topped peaks seen in the columns, even in the nonrelativistic limit, because when one is viewing the object perpendicular to the magnetic axis, so one can see both caps, the surface projection factors are very small (the effective visible surface is small), and this occurs near the

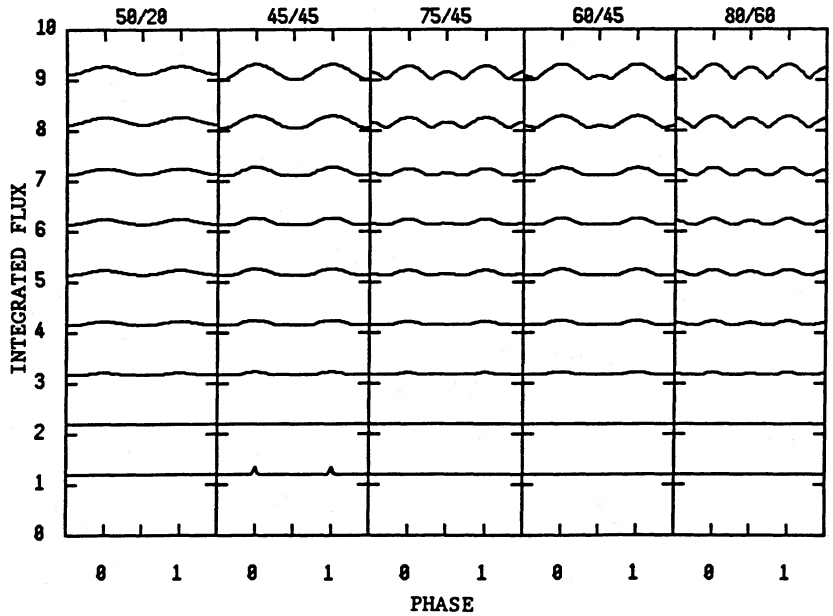

FIG. 7.—Polar cap bolometric pulse shapes for two poles and isotropic input emissivity function. Conventions as in Fig. 5

pulse minima, rather than near pulse maxima. Relativistic light bending does tend to fill in the minima, which tends to decrease the total modulation of cap models.

IV. RESULTS: FREQUENCY DEPENDENCE

In the polar-cap models, the frequency dependence is simple since all the radiation arises from the same stellar radius, and the observed spectrum can be obtained from the emitted spectrum by rescaling the frequency according to $\nu = \nu_0(1 - R_s/R)^{1/2}$. For the columns, however, at a fixed observed frequency ν one has contributions from a range of emitted frequencies $\nu(1 - R_s/R_c)^{-1/2} \leq \nu_0 \leq \nu(1 - R_s/R)^{-1/2}$. One gets a superposition of the emission function over all visible points on the surface, including multiple images, within this frequency range.

As the simplest example, we shall investigate here the response of the gravitational system to an input at the surface consisting of a delta function in frequency. That is, in equation (A10) we take

$$f_0(r_0, \mu_0, \phi_0, \nu_0) = g_0(r_0, \mu_0, \phi_0)\delta(\nu_0 - \nu_e) . \quad (9)$$

This type of function can be considered as a Green's function of the frequency-dependent emission problem; any realistic spectrum emitted from the column may be obtained by superposing such delta function inputs. To simplify things further, we take an angular distribution g_0, which is isotropic, but even so, one is still left with a rather complicated law of superposition of frequencies, due to the μ_0, ϕ_0 dependence of r_0, i.e., photons travel along paths of varying μ, ϕ. Using a numerical grid of 15 frequency points and 81 angle points, the spectral response function at the observer to a delta function frequency input at $\nu_0 = \nu_e$ is shown in Figure 8, for a single pole. The stellar radius is $R = 2.2R_S$, which is also the column lower radius, and the upper radius is $R_c = 2.38R_S$; again we have $\alpha = 5°$ and the resulting value of R_π is $2.34R_S$. The ordinate is

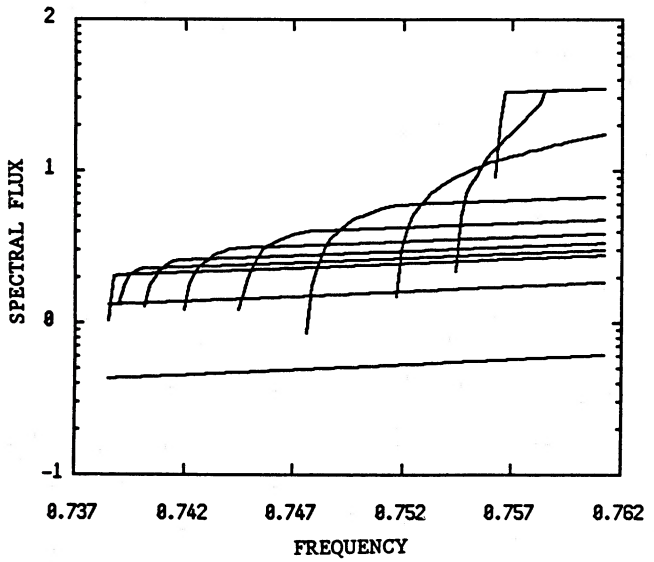

FIG. 8.—Observed differential spectral flux from a column with an emission function which is a delta function in frequency and isotropic in angle. Ordinate is flux [energy/(time frequency area)], and abscissa is observed frequency in units of input frequency at source. Bottom radius is $R = 2.2$, upper radius $R_c = 2.38$, and $R_\pi = 2.34$, $\alpha = 5°$. Various curves correspond to different observation angles Θ: 60°, 90°, 145°, 150°, 155°, 160°, 165°, 170°, 175°, 178°, 180° (from bottom tc top).

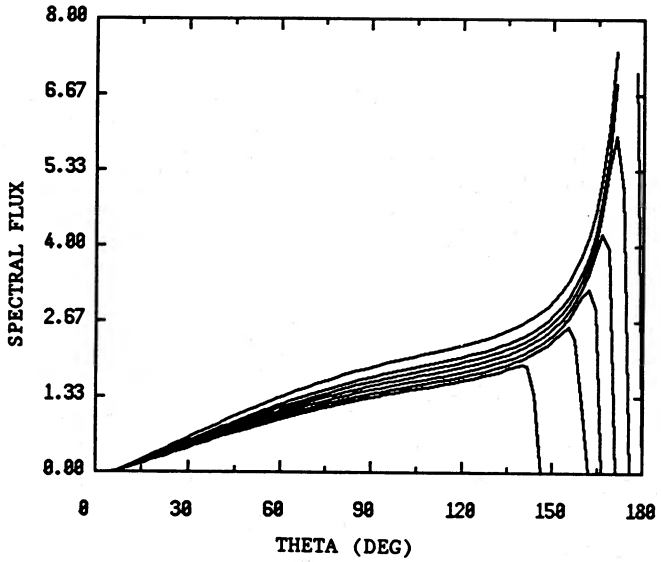

FIG. 9.—Beaming pattern at infinity for different observed frequencies, for a column with input source function which is a delta function in frequency and isotropic in angle. Ordinate is observed spectral flux [energy/(time frequency area)], and abscissa is observation angle θ, while different curves are for seven frequencies between lower and upper range of redshifted frequencies. Parameters are same as in Fig. 8.

the observed flux in arbitrary units, the abscissa is the observed frequency in units of the initial frequency ν/ν_e, and the various curves are for different angles Θ of observation. One sees that the (dimensionless) value of the emitted frequency $\nu_0/\nu_e = 1$ has been spread over a range of frequencies $\nu/\nu_e < 1$. Such effects ($\Delta\nu/\nu \approx 3\%$) would be resolvable experimentally, for example, with germanium detectors ($\Delta E/E \approx 1\%$). Due to the delta function nature of the injected spectrum, each observed frequency ν corresponds to a specific emission height r_0:

$$R \leq r_0 = \frac{\nu_e^2}{\nu_e^2 - \nu^2} R_S \leq R_c .$$

Thus, for the high frequencies ($\nu > 0.756\nu_e$) one has $r_0 > R_\pi$, which, for reasons outlined in the preceding paragraph, results in an enhanced flux for large observation angles Θ. It is seen from the spectral plot of Figure 8 that as Θ approaches π the bottom parts of the column are being increasingly obscured by the star leading to a cutoff in the spectrum at the corresponding frequencies.

The angular dependence of the observed flux for a set of fixed frequencies can be seen more clearly in the Figure 9. The fluxes for the lower frequencies (which originate closer to the bottom of the column) are cut off by the star at relatively "small" angles ($\Theta \approx 150°$–$165°$), and the high frequencies, corresponding to $r_0 > R_\pi$, are still visible at $\Theta = 180°$.

This frequency and angle-dependent emission structure has been translated into a more observationally familiar representation for rotating stars by plotting pulse shapes for a configuration of two oppositely located radiating columns. Figure 10 gives the normalized flux per unit frequency (ordinate) against pulse phase (abscissa), for eight different frequencies shown in increasing order from bottom to top and for various viewing angles shown along the top. Because the fluxes shown in Figure 8 are relatively slowly varying functions for a wide range of observation angles ($0 \leq \Theta < 140°$), not much pulsing is seen except for viewing angles which sample very close to the

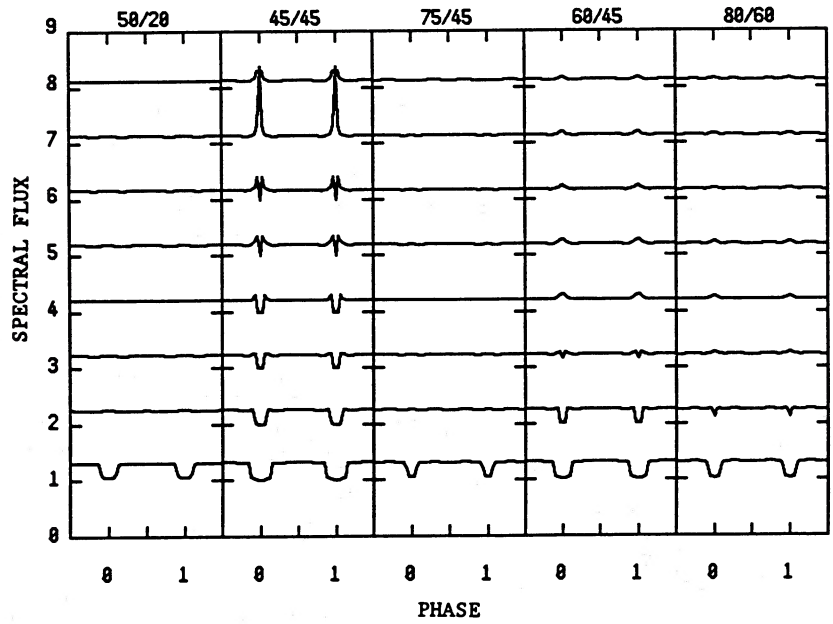

FIG. 10.—Column normalized pulse shapes for different frequencies observed, for two poles and an input emission function, which is a delta function in frequency and isotropic in angle. Various curves are for increasing freqeuency from bottom to top. Parameters are same as in Fig. 8.

polar axis, and which intersect the strongly backward bent beam. In the low-frequency case the obscured Θ-interval is large enough to give rise to the dips seen at phase 0 and 1 for all combinations i_1 and i_2. The fact that the flux for the high frequencies is beamed into a small interval at $\Theta = \pi$ leads to the peaks in Figure 9 for $i_1 = i_2 = 45°$. In this case, the pulse profiles are actually inverted if the pulses are observed in different energy bands.

V. DISCUSSION

We have calculated the frequency-dependent and frequency-integrated flux at infinity from columns and hot spots located on relativistic, slowly rotating neutron stars. These serve as models for isolated or binary accreting pulsars, assuming some simplified angular and frequency input spectrum at the emitting surface. Two isolated pulsars which show evidence of broadly modulated X-ray emission are PSR 1509−58 (e.g., Seward *et al.* 1983) and PSR 0540−693 (e.g., Middleditch and Pennypacker 1985), although this does not appear to be a widespread phenomenon for this class of sources (see Helfand and Becker 1984). By contrast, there are many accreting binary pulsar sources (see White, Swank, and Holt 1983).

The effect of gravitational light bending is rather large for configurations with radii less than ~ 2.5 Schwarzschild radii, both in the columns and the hot spots. For the latter case, our calculations are in agreement with Pechenick, Ftaclas, and Cohen (1983). We have used these hot-spot beam functions to present the actual pulse profiles as a function of pulse phase, which is the observed quantity, rather than the beam shape.

The major contribution of the present paper, however, is our calculation of the beams, pulse shapes, and spectral properties of a different type of emission region, generically labeled emission columns, or accretion columns in the case of accreting pulsars. The accretion columns distinguish themselves from the hot spots by a complicated mixing and shadowing behavior of the different frequencies, which appears due to the differential gravitational redshift. The column model contains an additional free parameter, namely the column's upper radius R_c. The general emission pattern at infinity, then, depends on whether this radius is larger or smaller than the characteristic radius $R_\pi(R, \alpha)$ defined in § III (a photon emitted at R_π such that its path grazes the stellar surface will be seen at an observation angle $\Theta = 180°$). For $R_c < R_\pi$, the star always obscures the column completely for large Θ, and, if $R_c > R_\pi$, a certain fraction of the column will be seen at $\Theta = 180°$, and, due to the large visible area, the flux is strongly enhanced in this direction. For small opening angles of the column ($\alpha < 10°$), the radius R_π increases rapidly with the stellar radius R; thus, for less relativisitic stars ($R > 10R_S$) one will usually have $R_c < R_\pi$. In general, one sees that both the column and the hot-spot beams are strongly backwardly bent for the most highly relativistic configurations. One might think that this could lead to an increase of the degree of modulation, since the beam is sharper. However, for the hot spots (caps), the observed flux arises from those rays that, at the surface, emerge close to $\Theta = 90°$, i.e., perpendicular to the B-field, and, for these directions, the effective surface area is very small (the usual limb-darkening law in flat space would be $F \propto \cos[\Theta]$), so that, in practice, this leads to a net decrease of the degree of modulation with decreasing radius for the hot-spot models (see Fig. 7). By contrast, for the column models, which are strongly backwardly bent, the effective surface area factor is much more favorable (corresponding to $F \propto \sin[\Theta]$ in the nonrelativistic limit), and the degree of modulation decreases more slowly with decreasing radius. For $R \leq 1.8R_S$, when the beam starts becoming very sharply backwardly bundled, a very sharp spike induced by the gravitational light bending appears in the pulse profiles for those viewing angles where the direction $\Theta \approx 180°$ is sampled (see Figs. 3 and 4). In addition, the columns studied here show an additional modulation, which is present even in the nonrelativistic limit, due to the fact that the "columns" considered here, unlike those of Nagel (1981) and Mészáros and Nagel (1985) are not cylinders but rather portions of cones, which are closer to the real dipole geometry (in the region

$\Delta R/R \leq 20\%$–30%) than are the cylinders. For cones of opening angle α, one can see both columns at the same time for $|\pi/2 - \theta| \leq \alpha$, which leads to a doubling of the visible flux. Thus, we find here that the column pulse shapes, even when strongly gravitationally bent, do not show a preferential lack of modulation compared to the hot-spot (or slab) models. We have also investigated, but not presented here, more beamed angular injection functions, such as might be expected from scattering atmospheres. The resulting light curves are only modestly more modulated than those in the results of Figures 3–7.

We have presented a formalism for investigating the frequency changes of an arbitrary input spectrum as it propagates to infinity from points on the surface of a column above the stellar surface and have calculated examples involving an input delta function in frequency, whose response at infinity is the Green's function of the problem. Subtle effects arise due to the shadowing of different frequency contributions, arising from different heights, by the stellar surface and by the opposite column, or by the same column after a full rotation, especially in the more extreme relativistic cases. In general, the lower frequencies, which arise from closer to the surface, are the ones that suffer most shadowing, which appears beyond a certain angle. This leads to the interesting phenomenon apparent in Figure 8, showing a peak at the higher frequencies (where the radiation is not shadowed provided the upper column radius R_c is greater than the characteristic radius R_π) and a trough at low frequencies (where shadowing has occurred). This may provide a different explanation for some of the pulse shape "inversions" detected in some X-ray pulsars, such as GX 1+4 and 4U 1626−67 (see White, Swank, and Holt 1983). For an alternative explanation, see Mészáros and Nagel (1985) and White, Swank, and Holt (1983).

The injection models investigated here are of the simplest kind, in order to distinguish between the purely gravitational or geometrical effects and those effects which are connected with the physics of the surface layers or the radiative transfer. The delta function frequency input discussed can be used either as a Green's function, to calculate the response of any arbitrary input frequency spectrum, or may be considered as a very simplified model of a spectral line, e.g., a cyclotron line or a heavy-element resonance line. In a subsequent publication, we shall present results of light bending in columns and hot spots using as an input the magnetic radiative transfer calculations for the corresponding geometries.

We are grateful to W. Nagel for useful discussions concerning hot spots and to C. Ftaclas for many comments which helped improve the manuscript. This research has been partially supported by the Deutsche Forschungsgemeinschaft and by NSF grant 85-14735.

APPENDIX A

COLUMN EQUATIONS

The radiating surface of the column is taken to be given by the section of the conical surface

$$R \leq r_0 \leq R_c, \qquad \Theta_0 = \alpha = \text{constant}, \qquad 0 \leq \Phi_0 \leq 2\pi , \tag{A1}$$

where R and R_c are the lower and upper column radii. Here, we assume that the lower boundary also agrees with the stellar surface. Some of the radiation emitted will fall upon the star and will not be observed. This is taken into account by specifying the emission function f_0,

$$f_0 = 0 , \quad \text{for } \mu_0 < \mu_R, \text{ all } \phi_0, \nu_0, \text{ and } r_0, \Theta_0, \Phi_0 \text{ given by equation (8)} ,$$

where μ_R follows from equation (4a) with $r = R$ and $\mu = 0$, and radii in Schwarzschild units,

$$\mu_R = -\left(1 - \frac{R^2}{r_0^2}\frac{1 - 1/r_0}{1 - 1/R}\right)^{1/2} . \tag{A2}$$

In addition, for strongly bent rays, the photon may hit the same column at the opposite side of the emission point if the deflection angle becomes

$$K(r, r_0, \mu_0) = 2(\pi - \alpha), \qquad r < R_c .$$

We define the quantity μ_c by the implicit relation

$$K(R_c, r_0, \mu_c) = 2(\pi - \alpha), \qquad \text{one pole} , \tag{A3}$$

or, for a second pole, by $K(R_c, r_0, \mu_c) = \pi - 2\alpha$. Both effects described above can be represented by the requirement

$$f_0 = 0 , \quad \text{for } \mu_0 < \mu_L, \text{ all } \phi_0, \nu_0, \text{ and } r_0, \Theta_0, \Phi_0 \text{ given by equation (A1)} , \tag{A4}$$

where $\mu_L = \max(\mu_R, \mu_c)$. A further restriction on f_0 is the condition that the column radiates only in the outward direction,

$$f_0 = 0 , \quad \text{for } \cos\phi_0 < 0, \text{ all } \mu_0, \nu_0, \text{ and } r_0, \Theta_0, \Phi_0 \text{ given by equation (A1)} . \tag{A5}$$

In addition, we require the symmetry relation

$$f_0(\phi_0) = f_0(2\pi - \phi_0) , \tag{A6}$$

which means there is no flux in the Φ-direction.

We now calculate the Jacobian appearing in equation (3). Since $\Theta_0 = \alpha$ is constant in our case, equation (4b) shows that ϕ depends on ϕ_0 only (since the observer's r, Θ, Φ are fixed for these considerations). Therefore,

$$\mu D = \mu \frac{\partial \mu}{\partial \mu_0} \frac{\partial \phi}{\partial \phi_0} ,$$

and, from equation (4b), we have

$$\frac{\partial \phi}{\partial \phi_0} = \frac{\sin \alpha \cos \phi_0}{(\sin^2 \Theta - \sin^2 \alpha \sin^2 \phi_0)^{1/2}} . \tag{A7}$$

For the calculation of $\mu(\partial\mu/\partial\mu_0)$ from equation (4a), one has to keep in mind that r_0 depends on ϕ_0, μ_0. From equation (4a) we have

$$\mu \frac{\partial \mu}{\partial \mu_0} = \left(\frac{Ar_0}{A_0 r}\right)^2 \left[\mu_0 - \frac{A_0}{r_0}(1 - \mu_0^2) \frac{\partial}{\partial \mu_0}\left(\frac{r_0}{A_0}\right)\right] . \tag{A8}$$

Differentiating the relation of equation (4e) with respect to μ_0 leads to $\partial K/\partial \mu_0 = 0$, and, from equation (5), we obtain the last derivative in equation (A8), so that

$$\mu \frac{\partial \mu}{\partial \mu_0} = \frac{1}{r^2} \frac{r_0^2}{r_0 - 3/2} \frac{1}{Y(r_0, \mu_0)} , \tag{A9}$$

where

$$Y(r_0, \mu_0) = \int_{r_0}^{\infty} q(x, b)\, dx + \begin{cases} 0 , & \text{for } \mu_0 \geq 0, \\ 2 \displaystyle\int_{r_m}^{r_0} q(x, b)\, dx , & \text{for } \mu_0 < 0 , \end{cases}$$

with

$$q(x, b) = \frac{x - 3/4}{x(x - 3/2)^2} [x^2 - b^2(1 - 1/x)]^{-1/2} ,$$

with $r \to \infty$ assumed in the expression for K. The spectral flux may now be written as

$$F_\nu(r, \Theta) = 2 \frac{\nu^3}{r^2} \iint_{S_0} \frac{\cos \phi_0}{[\eta^2 - \sin^2 \phi_0]^{1/2}} \frac{r_0^2}{r_0 - 3/2} \frac{1}{Y(r_0, \mu_0)} f_0(r_0, \mu_0, \phi_0, \nu_0) d\mu_0\, d\phi_0 , \tag{A10}$$

where S_0 is the region of ϕ_0, μ_0, where $f_0 \neq 0$ and $\eta = \sin \Theta/\sin \alpha$ and $\nu_0 = \nu(1 - 1/r_0)^{-1/2}$. The factor 2 stems from the symmetry relation of equation (A6), and ϕ_0 is restricted to the range $0 \leq \phi_0 < \pi/2$. An equivalent procedure can be applied for obtaining the frequency-integrated flux,

$$F(r, \Theta) = \int_0^{\infty} F_\nu\, d\nu ,$$

and one obtains

$$F(r, \Theta) = \frac{2}{r^2} \iint_{S_0} \frac{\cos \phi_0}{(\eta^2 - \sin^2 \phi_0)^{1/2}} \frac{r_0^2 - 1}{r_0 - 3/2} \frac{1}{Y(r_0, \mu_0)} I_0(r_0, \mu_0, \phi_0)\, d\mu_0\, d\phi_0 , \tag{A11}$$

in which the intensity $I_0 = \int_0^{\infty} \nu_0^3 f_0\, d\nu_0$ is a given function at the column. The additional factor $(1 - 1/r_0)^2$ in the integral is a result of the frequency transformation.

To complete the equations, we must still calculate explicitly the region of integration S_0 in the ϕ_0, μ_0 plane. First, the condition of equation (A5) can be used to constrain the function K. From equation (4e), using the fact that $0 \leq \cos \phi_0 \leq 1$, we get

$$\begin{aligned} 2\pi(n + 1) + \Theta - \alpha \leq K \leq 2\pi(n + 1) + \Theta + \alpha ; &\quad \text{for } 0 \leq \Theta \leq \alpha , \\ 2\pi n + \Theta - \alpha \leq K \leq 2\pi n + \beta , &\quad \text{for } \alpha \leq \Theta \leq \pi - \alpha , \\ 2\pi(n + 1) - \Theta - \alpha \leq K \leq 2\pi(n + 1) - \beta , &\quad \text{for } \alpha \leq \Theta \leq \pi - \alpha , \\ 2\pi n + \Theta - \alpha \leq K \leq 2\pi(n + 1) - \Theta - \alpha , &\quad \text{for } \pi - \alpha \leq \Theta \leq \pi , \end{aligned} \tag{A12}$$

where $\beta = \arccos(\cos \Theta/\cos \alpha)$, and multiple images are taken into account through the integer $n = 0, 1, 2, \ldots,$. The relation (4e)

also allows the representation of K as a function of ϕ_0,

$$\cos\,[K(\infty, r_0, \mu_0)] = \cos\,[h_\pm(\phi_0)]\,,$$

$$h_\pm(\phi_0) = \arccos\left[\frac{1}{1-\sin^2\alpha\,\sin^2\phi_0}(\cos\Theta\cos\alpha \pm \sin^2\alpha\cos\phi_0(\eta^2-\sin^2\phi_0)^{1/2}\right]. \tag{A13}$$

Assuming $r_0 = R$ and $r_0 = R_c$, this relation implicitly defines the boundaries of the μ_0 integration, which then depends on ϕ_0. The integral (A10) can now be written as

$$F_\nu = \frac{2\nu^3}{r^2}\sum_{n=0}^{N}\int_0^{\phi_B}\frac{\cos\phi_0}{(\eta^2-\sin^2\phi_0)^{1/2}}\left(\int_{a_n^+}^{b_n^+}\Psi\,d\mu_0 + \int_{a_n^-}^{b_n^-}\Psi\,d\mu_0\right)d\phi_0\,, \tag{A14}$$

where

$$\Psi(r_0, \mu_0, \phi_0, \nu_0) = \frac{r_0^2}{r_0 - 3/2}\frac{1}{Y(r_0,\mu_0)}f_0\,,$$

and the boundaries are given by $\phi_B = \pi/2$ for $\alpha \le \Theta \le \pi - \alpha$, $\phi_B = \arcsin(\sin\Theta/\sin\alpha)$ in all other cases, (from the root of eq. [A13]), and $a_n^\pm = \min[\mu_L(r_\pm), \gamma_n^\pm]$, $b_n^\pm = \min[\mu_L(r_\pm), \lambda_n^\pm]$. This takes into account the possibility that the photons can be absorbed by the star or the column. The quantities $\gamma_n^\pm$, $\lambda_n^\pm$, and $r_\pm$ are implicitly defined by

$$K(\infty, R_c, \gamma_n^\pm) = w_n^\pm\,, \qquad K(\infty, R, \lambda_n^\pm) = w_n^\pm\,, \qquad K[\infty, r_\pm, \mu_L(r_\pm)] = w_0^\pm\,,$$

where $w_n^\pm$ [which contains the function $h_\pm(\phi_0)$] can be deduced from the limits defined by equation (A12),

$$w_n^\pm = \begin{cases} 2\pi(n+1) - h_\pm\,, & \text{for } 0 \le \Theta \le \alpha\,, \\ 2\pi n + h_\pm\,, & \text{for } \pi - \alpha \le \Theta \le \pi\,, \end{cases}$$

and

$$w_n^+ = 2\pi n + h_+\,,$$

$$w_n^- = 2\pi(n+1) - h_-\,, \qquad \text{for } \alpha \le \Theta \le \pi - \alpha\,.$$

The sum appearing in the final part of equation (A14) counts the multiple images, and the number of images N is determined by the maximum possible deflection angle $K_{\max} = K[\infty, R_c, \mu_L(R_c)]$, i.e., N is the smallest integer greater than $K_{\max}/2\pi - 1$. In the integrals of equation (A14), r_0 is a function of μ_0, ϕ_0, which must be determined from

$$K(\infty, r_0, \mu_0) = w_n^\pm(\phi_0)\,.$$

The integrals for the flux were solved numerically. We checked our numerical scheme by calculating the total luminosity in two different ways and comparing results. Integrating the transport equation (1) over the solid angle $d\mu\,d\phi$ leads to a conservation law for the integrated flux $\boldsymbol{F} = \int_{4\pi}\int_0^\infty \boldsymbol{n}\omega^3 f\,d\mu\,d\phi\,d\omega$:

$$\frac{A}{r^2}\frac{\partial}{\partial r}(r^2A^2F_r) + \frac{A^2}{r\sin\Theta}\frac{\partial}{\partial\Theta}(\sin\Theta F_\Theta) = 0\,. \tag{A15}$$

From Gauss's theorem, one can deduce the following expression for the total luminosity L_∞, appropriate to the emission region under consideration,

$$L_\infty = 2\pi r^2\int_0^\pi \sin\Theta F_r(r,\Theta)d\Theta = 2\pi\sin\alpha\int_R^{R_c} r_0(1-1/r_0)^{1/2}F_\Theta(r_0,\alpha)dr_0\,, \tag{A16}$$

where the first integral is calculated over a remote sphere of radius r and the second one extends over our conical emission region. Taking F_r from the equation (A11) and comparing the above two integrals, we always obtained a relative error of the order of 10^{-3}–10^{-4}.

APPENDIX B

CAP EQUATIONS

We consider here the case of a radiating polar cap defined by

$$r_0 = R = \text{constant}\,, \qquad 0 \le \Theta_0 \le \alpha\,, \qquad 0 \le \Phi_0 \le 2\pi\,. \tag{B1}$$

The derivation of an equation for the observed flux is very similar to the method outlined in Appendix A, and we therefore give this derivation very briefly without going into the details.

The star will absorb all photons emitted with $\mu_0 < 0$; thus, we have

$$f_0 = 0, \quad \text{for } \mu_0 < 0, \text{ all } \phi_0, \nu_0, \text{ and } r_0, \Theta_0, \Phi_0 \text{ given by (B1)}\,.$$

The angle K is now given by equation (5a) with $Q = 0$ throughout, and it depends on μ_0 only because $r_0 = R$ is constant. The Jacobian is again given by

$$\mu D = \mu \frac{\partial \mu}{\partial \mu_0} \frac{\partial \phi}{\partial \phi_0} ,$$

with

$$\mu \frac{\partial \mu}{\partial \mu_0} = \left(\frac{R}{r}\right)^2 \frac{1}{1 - 1/R} \mu_0 , \qquad \frac{\partial \phi}{\partial \phi_0} = \frac{\sin \Theta_0}{\cos \phi \sin \Theta} \frac{\cos \Theta_0 \sin K + \cos \phi_0 \cos K \sin \Theta_0}{\sin \Theta_0 \cos K + \cos \phi_0 \sin K \cos \Theta_0} ,$$

and the relations (4b) and (4e) must be used to express ϕ and Θ_0 in terms of ϕ_0, Θ, and $K(\infty, R, \mu_0)$. Assuming again the symmetry relation (A6), the flux F_ν reads

$$F_\nu(r, \Theta) = 2\nu^3 \left(\frac{R}{r}\right)^2 \frac{1}{1 - 1/R} \iint_{S_0} \frac{\partial \phi}{\partial \phi_0} f_0(\Theta_0, \mu_0, \phi_0, \nu_0) \mu_0 \, d\mu_0 \, d\phi_0 \tag{B2}$$

(note that Θ_0 must be considered as a function of μ_0 due to eq. [4e]).

For the case that the emitted radiation field is independent of ϕ_0, the corresponding integration can be performed easily using the restriction $\Theta_0 \leq \alpha < \pi/2$:

$$F_\nu(r, \Theta) = 2\nu^3 \left(\frac{R}{r}\right)^2 \frac{1}{1 - 1/R} \int_0^1 \phi_L(\alpha, \Theta, \mu_0) f_0(\Theta_0, \mu_0, \nu_0) \mu_0 \, d\mu_0 , \tag{B3}$$

where

$$\phi_L = \begin{cases} \arccos(B) , & -1 \leq B \leq 1 , \\ 0 , & B > 1, \\ \pi , & B < -1 , \end{cases} \tag{B4}$$

and

$$B = \frac{\cos \alpha - \cos \Theta \cos K}{\sin \Theta \sin K} .$$

From this we obtain for the integrated flux

$$F(r, \Theta) = 2\left(\frac{R}{r}\right)^2 \left(1 - \frac{1}{R}\right) \int_0^1 \phi_L(\alpha, \Theta, \mu_0) I_0(\Theta_0, \mu_0) \mu_0 \, d\mu_0 , \tag{B5}$$

which corresponds to the result derived recently by Pechenick, Ftaclas, and Cohen (1983).

REFERENCES

Alme, M. L., and Wilson, J. R. 1973, *Ap. J.*, **186**, 1015.
Arons, J. 1981, *Ap. J.*, **248**, 1099.
Basko, M. M., and Sunyaev, R. A. 1976, *M.N.R.A.S.*, **175**, 395.
Cheng, A. F., and Ruderman, M. 1980, *Ap. J.*, **235**, 576.
Davidson, K. 1973, *Nature Phys. Sci.*, **246**, 1.
Ftaclas, C., Kearney, M. W., and Pechenick, K. R. 1986, *Ap. J.*, **300**, 203.
Harding, A. K., Mészáros, P., Kirk, J. G., and Galloway, D. J. 1984, *Ap. J.*, **278**, 369.
Helfand, D. J., and Becker, R. H. 1984, *Nature*, **307**, 215.
Helfand, D. J., Chanan, G. A., and Novick, R. 1980, *Nature*, **283**, 336.
Kirk, J. G. 1984, *Astr. Ap.*, **142**, 130.
Lindquist, R. W. 1966, *Ann. Phys.*, **37**, 487.
Mészáros, P. 1984, *Space Sci. Revs.*, **38**, 325.
Mészáros, P., Harding, A. K., Kirk, J. G., and Galloway, D. J. 1983, *Ap. J. (Letters)*, **266**, L33.
Mészáros, P., and Nagel, W. 1985, *Ap. J.*, **299**, 138.
Middleditch, J., and Pennypacker, C. R. 1985, *Nature*, **313**, 659.
Misner, C. W., Thorne, K. S., and Wheeler, J. A. 1973, *Gravitation*, (San Francisco: Freeman).
Nagel, W. 1981, *Ap. J.*, **251**, 288.
Pechenick, K. R., Ftaclas, C., and Cohen, J. M. 1983, *Ap. J.*, **274**, 846.
Riffert, H. 1986, *Ap. J.*, **310**, 729.
Seward, F. D., Harnden, F. R., Murdin, P., and Clark, D. H. 1983, *Ap. J.*, **267**, 698.
Shapiro, S. L., and Teukolsky, S. L. 1983, *Black Holes, White Dwarfs, and Neutron Stars*, (New York: Wiley-Interscience).
Wang, Y-M., and Frank, J. H. 1981, *Astr. Ap.*, **93**, 255.
White, N. E., Swank, J. H., and Holt, S. S. 1983, *Ap. J.*, **270**, 711.
Zel'dovich, Ya. B., and Shakura, N. I. 1969, *Soviet Astr.—AJ*, **13**, 175.

P. Mészáros: Pennsylvania State University, Department of Astronomy, 525 Davey Laboratory, University Park, PA 16082

H. Riffert: JILA, University of Colorado, Box 440, Boulder, CO 80309